Facile Synthesis and Luminescence Properties of Highly Uniform MF/YVO 4 :Ln 3+ (Ln = Eu, Dy, and Sm) Composite Microspheres

ARTICLE *in* CRYSTAL GROWTH & DESIGN · AUGUST 2009

Impact Factor: 4.89 · DOI: 10.1021/cg9004104

5 AUTHORS, INCLUDING:

Guang Jia
Hebei University
70 PUBLICATIONS **1,571** CITATIONS
SEE PROFILE

Yujie Lu
University of Texas Medical School
79 PUBLICATIONS **1,499** CITATIONS
SEE PROFILE

Yanhua Song
Jilin University
88 PUBLICATIONS **1,842** CITATIONS
SEE PROFILE

Hongpeng You
Chinese Academy of Sciences
178 PUBLICATIONS **3,414** CITATIONS
SEE PROFILE

CRYSTAL GROWTH & DESIGN
2009
VOL. 9, NO. 8
3702–3706

Facile Synthesis and Luminescence Properties of Highly Uniform $MF/YVO_4:Ln^{3+}$ (Ln = Eu, Dy, and Sm) Composite Microspheres

Guang Jia, Kai Liu, Yuhua Zheng, Yanhua Song, and Hongpeng You*

State Key Laboratory of Rare Earth Resource Utilization, Changchun Institute of Applied Chemistry, Chinese Academy of Sciences, Changchun 130022, and Graduate University of the Chinese Academy of Sciences, Beijing 100049, P. R. China

Received April 11, 2009; Revised Manuscript Received May 16, 2009

ABSTRACT: Uniform $MF/YVO_4:Ln^{3+}$ (Ln = Eu, Dy, and Sm) composite microspheres have been prepared via a simple and economical wet-chemical route at ambient pressure and low temperature. Monodisperse micrometer-sized melamine formaldehyde (MF) colloidal particles were first fabricated by a condensation process of melamine with formaldehyde. Subsequently, well-dispersed YVO_4 nanoparticles were successfully grown onto the MF microspheres to form core−shell structured composite particles in aqueous solution. The as-obtained composite microspheres with perfect spherical shape are uniform in size and distribution, and the thickness and roughness of the YVO_4 shells on MF cores could be tuned by varying the reaction temperature. The $MF/YVO_4:Ln^{3+}$ composite phosphors show strong light emissions with different colors coming from different activator ions under ultraviolet excitation, which might find potential applications in fields such as light phosphor powders and advanced flat panel displays.

1. Introduction

Over the past few years, the synthesis of heterostructures with core−shell architecture has attracted considerable attention in materials chemistry and nanotechnology due to the ability to tune their properties.[1,2] Coating the particles with a thin shell of a compatible material makes it possible to control the interparticle and particle−matrix interactions, thereby further improving functional properties and expanding to a broader range of potential applications. The structure, size, and composition of these particles can be altered easily in a controllable way to tailor their magnetic, optical, mechanical, thermal, electrical, electrooptical, or catalytic properties.[3−5] Recently, the core−shell structured particles with spherical morphology have been interestingly studied due to their potential applications in photonic crystals, catalyst, photonics, and biological labeling.[6−10] The size and dispersibility of the spherical core−shell structured materials are dependent on the spherical cores. As we know, polystyrene (PS) and silica (SiO_2) beads have been reported to serve as effective templates for the preparation of core−shell composite particles because of their simple preparation, ease in surface functionalization, and flexibility in size variations.[5,11−17] Recently, the melamine formaldehyde (MF) colloidal particles which act as a template have been steadily employed to fabricate hollow silica and Fe_2O_3 spheres,[18,19] carbon spheres,[20,21] and functionalized polyelectrolyte multilayer-coated particles or hollow capsules.[22−24] However, to the best of our knowledge, no report has been devoted to the preparation of core−shell structured luminescent materials by using MF colloidal particles as a template.

On the other hand, phosphor particles with spherical morphology, nonaggregation, and narrow size distribution can improve the optical performance because of the high packing density and the reduction of light scattering.[25,26] Nowadays, many synthetic routes have been developed to control the size and distribution of phosphor particles, such as spray pyrolysis[27] and fluxes precipitation,[28] but the obtained phosphor particles are still far from the ideally monodisperse spherical morphology. It seems to be a promising way to fabricate ideal spherical phosphor particles by incorporating the luminescent nanocrystals onto the surface of spherical template. However, most nanocrystalline luminescent materials are prepared at high temperature and are not dispersible in water, which makes it difficult to incorporate them onto the spherical template uniformly.

In this work, we have developed a simple, surfactant-free, and efficient approach to grow luminescent lanthanide ion doped YVO_4 nanocrystals onto melamine formaldehyde colloid particles to form a core−shell structure with a narrow size distribution. The monodisperse core−shell structured phosphors show strong light emissions with different colors by changing the lanthanide ions doped into the YVO_4 nanocrystals. Furthermore, the core−shell phosphor materials will be cheaper than the pure phosphor materials in unit mass because melamine formaldehyde resin is cheaper than most of the phosphor materials which often employ expensive rare-earth elements as activators and/or host components.

2. Experimental Section

The rare earth oxides (99.99%) were purchased from Wuxi Yiteng Rare-Earth Limited Corporation (China), and other chemicals were purchased from Beijing Chemical Corporation. All the other chemicals were analytical grade reagents and were used directly without further purification. $Ln(NO_3)_3$ (Ln = Y, Eu, Dy, and Sm) aqueous solutions were obtained by dissolving Ln_2O_3 in dilute HNO_3 solution under heating with agitation.

2.1. Synthesis of Monodisperse MF Microspheres. In a typical synthesis, a solution of formaldehyde (9.8 g, 37%) and deionized water (200 mL) was prepared and heated to 60 °C. Subsequently, 2.5 g of melamine was added with stirring. When the melamine was completely dissolved, formic acid was introduced to the vigorously stirred solution until pH = 5. The transparent solution turned turbid by stirring for about 20 min. After additional agitation of the solution for 20 min, the obtained white colloidal particles were washed several times with deionized water and absolute ethanol and dried at 60 °C in air.

2.2. Synthesis of $MF/YVO_4:Eu^{3+}$ Composite Particles. In the preparation procedure, 2 mmol of NH_4VO_3 was added to 40 mL of deionized water and the obtained mixture was stirred vigorously for 10 min. NaOH solution (2 M) was then introduced to the stirred solution until pH = 13 to form a clear solution. The as-prepared MF microspheres (0.2 g) were added and well dispersed into the above solution with the assistance of ultrasonication for 10 min. Subsequently, a solution of 1.9 mmol of $Y(NO_3)_3$ and 0.1 mmol of $Eu(NO_3)_3$ in 40

* To whom correspondence should be addressed. E-mail: hpyou@ciac.jl.cn.

10.1021/cg9004104 CCC: $40.75
Published on Web 06/08/2009

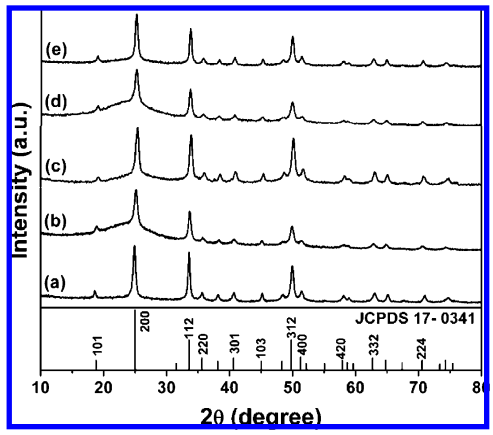

Figure 1. X-ray diffraction patterns of pure YVO_4:Eu^{3+} prepared at 70 °C (a), core−shell structured MF/YVO_4:Eu^{3+} composite particles prepared at 70 °C (b) and 90 °C (c), MF/YVO_4:Dy^{3+} (d) and MF/YVO_4:Sm^{3+} (e) samples prepared at 70 °C. The standard data for tetragonal phase YVO_4 (JCPDS No. 17-0341) is presented in the figure for comparison.

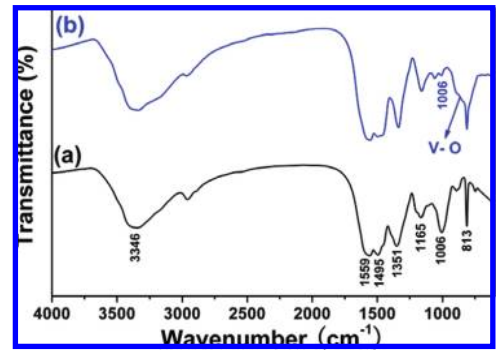

Figure 2. FT-IR spectra of (a) pure MF microspheres and (b) MF/YVO_4:Eu^{3+} composite particles.

mL of deionized water was added into the above colloidal solution dropwise. The resultant mixture was heated to 70 or 90 °C for 2 h with vigorous stirring. The final products were washed by deionized water and ethanol several times respectively and dried at 60 °C in air.

For comparison, the pure nanocrystalline YVO_4 sample was synthesized using the same method in the absence of the MF template. A similar process was employed to prepare Dy^{3+} and Sm^{3+}-doped MF-YVO_4 composite microspheres (3 mol %) by using $Dy(NO_3)_3$ and $Sm(NO_3)_3$ solutions instead of $Eu(NO_3)_3$ solution as described above.

2.3. Characterization. The samples were characterized by powder X-ray diffraction (XRD) performed on a D8 Focus diffractometer (Bruker). Fourier transform infrared spectroscopy (FT-IR) spectra were measured with a Perkin-Elmer 580B infrared spectrophotometer with the KBr pellet technique. The morphology and composition of the samples were inspected using a scanning electron microscope (SEM; S-4800, Hitachi) equipped with an energy-dispersive X-ray spectrum (EDX; XFlash-Detector 4010, Bruker). Transmission electron microscopy (TEM) images and selected area electron diffraction (SAED) patterns were obtained using a JEOL 2010 transmission electron microscope operating at 200 kV. Samples were prepared by placing a drop of a dilute alcoholic dispersion of products on the surface of a silicon substrate or a copper grid for SEM and TEM measurements. Photoluminescence (PL) excitation and emission spectra were recorded with a Hitachi F-4500 spectrophotometer equipped with a 150 W xenon lamp as the excitation source. The luminescence decay curves were obtained from a Lecroy Wave Runner 6100 Digital Oscilloscope (1 GHz) using a tunable laser (pulse width = 4 ns, gate = 50 ns) as the excitation (Contimuum Sunlite OPO). All measurements were performed at room temperature.

3. Results and Discussion

3.1. Phase Identification, Morphology, and Formation Mechanism of As-Obtained MF/YVO_4:Eu^{3+} Composite Particles. Figure 1 shows the XRD patterns of the as-synthesized pure YVO_4:Eu^{3+} (a), core−shell structured MF/YVO_4:Eu^{3+} samples prepared at 70 °C (b) and 90 °C (c), MF/YVO_4:Dy^{3+} (d), and MF/YVO_4:Sm^{3+} (e) samples prepared at 70 °C, respectively. The diffraction peaks of all the five samples can be well indexed to the tetragonal phase of YVO_4 (JCPDS No. 17-0341). No additional peaks of other phases can be detected, indicating that the pure tetragonal phase YVO_4 has formed, and the activator ions (Eu^{3+}, Dy^{3+}, and Sm^{3+}) have been effectively doped into the YVO_4 host lattice. Furthermore, it can be seen from Figure 1 that all the diffraction peaks shift a little to a lower angle in comparison with the standard data for tetragonal phase YVO_4. The spectral shift of the diffraction peaks can be explained by the doping activator ions. When the Y^{3+} ions were substituted by Eu^{3+}, Dy^{3+}, or Sm^{3+} ions with bigger radii, the crystal lattice constants as well as *d*-spacing increased, and thus the diffraction angles decrease due to the Bragg equation.

The reaction of melamine with formaldehyde leads to hydroxymethylation, whereas hydrogen atoms in the NH_2 groups of the melamine are substituted by methylol groups (CH_2OH), followed by cross-linking of the resulting methylolmelamines. Some different functional groups can appear depending on the degree of cross-linking, which is controlled by the reaction conditions. FT-IR spectra were used to identify the functional groups of the as-obtained MF microspheres and the core−shell structured composite particles. It can be seen from Figure 2a that the as-synthesized MF particles show the characteristic absorption bands of MF resins, which are similar to some previous reports.[18,20,29] The absorption bands at 3346, 1495 (1595), 1351, 1165, 1006, and 813 cm^{-1} are assigned to the vibration of hydroxy/amino (-OH/-NH_2), amino (-NH_2), amino, amine (C−N), ether (C−O−C), and C−N−C groups, respectively. This result indicates the formation of the MF resins. The FT-IR spectrum of core−shell structured composite particles (Figure 2b) is similar to that of the pure MF sample. However, it can be observed clearly that the IR band of ether groups (1006 cm^{-1}) becomes weaker, which may be caused by the coating of the nanoparticles on the surfaces of MF template. In addition, one can see that the sharp absorption peak of C−N−C groups (813 cm^{-1}) becomes broader (Figure 2b). The broadband is assigned to the combination for the vibration of C−N−C groups and the characteristic mode of V−O bonds (from VO_4^{3-} groups).[17,30,31] This result provides additional evidence for the formation of the YVO_4 nanoparticles on the surfaces of MF microspheres.

Figure 3a is a SEM image of the as-obtained pure YVO_4:Eu^{3+} sample prepared at 70 °C without MF microspheres as a template. The SEM image clearly shows that the sample consists of uniform spindle-like nanoparticles with equatorial diameters of 30−50 nm and lengths of 80−120 nm. Figure 3b shows the energy dispersive X-ray (EDX) spectrum analysis of the nanocrystalline YVO_4:Eu^{3+} sample. It confirms the presence of yttrium (Y), oxygen (O), vanadium (V), and europium (Eu) elements in the YVO_4:Eu^{3+} sample. No other impurity peaks can be detected, which can effectively support the XRD results of the sample.

Figure 4 shows the detailed SEM images of the as-formed bare MF microspheres and the core−shell structured composite particles. It can be seen from Figure 4a that the well-dispersed bare MF template consists of highly uniform microspheres with diameters of about 2.5 μm. It can also be observed that the

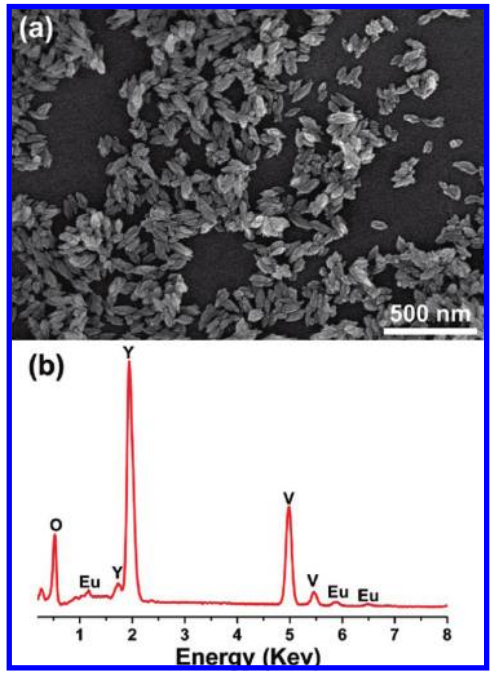

Figure 3. (a) SEM image and (b) EDX spectrum of pure $YVO_4:Eu^{3+}$ sample prepared at 70 °C without MF particles as a template.

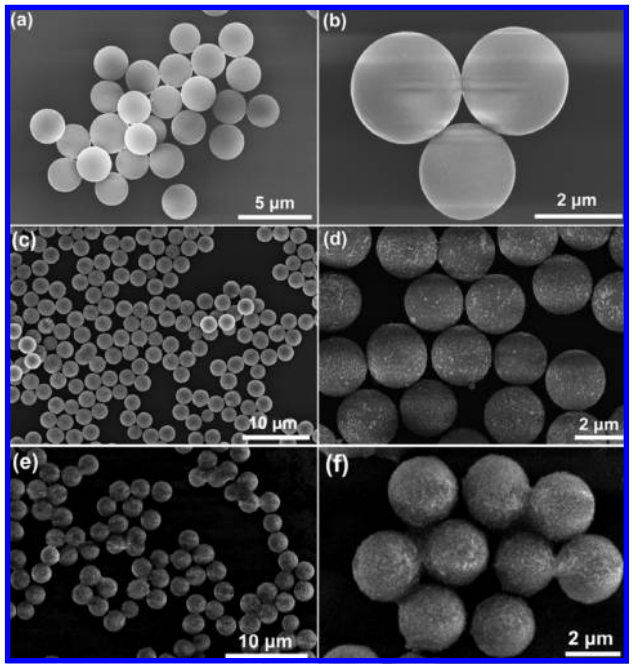

Figure 4. SEM images of pure MF microspheres (a, b), and core−shell structured $MF/YVO_4:Eu^{3+}$ composite particles prepared at 70 °C (c, d) and 90 °C (e, f).

surfaces of monodisperse MF microspheres are very smooth from the enlarged SEM image (Figure 4b). After functionalizing the MF microspheres by the YVO_4 nanoparticles (70 °C), the resulting MF/YVO_4 composite particles still keep the morphological properties of the pure MF microspheres; that is, these particles are still spherical and nonaggregated. We can also clearly see that the numerous individual and uniform nanodots spread around the surfaces of MF microspheres, indicating that the well-dispersed YVO_4 nanoparticles decorate the colloidal MF surface quite uniformly (Figure 4c,d). In addition, the morphologies of the $MF/YVO_4:Dy^{3+}$ and $MF/YVO_4:Sm^{3+}$ composite microspheres are the same as for the $MF/YVO_4:Eu^{3+}$ sample (not shown here).

The MF colloidal microspheres were prepared in aqueous solution and consist of a large amount of hydrophilic functional groups, which can be confirmed by the FT-IR spectra (Figure 2). Therefore, the MF templates are hydrophilic and may have a good affinity with VO_4^{3-} and Y^{3+} in aqueous solution. It is believed that the YVO_4 nuclei which formed in reaction media were absorbed on the surface of hydrophilic MF beads during the formation of the composite particles. This nucleation process is followed by growth of the formed nuclei until the supersaturation state is achieved. With the reaction proceeding at a designed temperature, YVO_4 nuclei continued to grow and served as the seeds for the growth of YVO_4 nanoparticles on the surface of the MF templates, resulting in the core−shell structured composite microspheres.

By increasing the reaction temperature to 90 °C, the YVO_4 nanocrystallites are concentrated and densely distributed on the surfaces of MF microspheres. The surfaces of the as-synthesized composite particles become rougher and the YVO_4 shells become thicker (Figure 4e,f). In addition, the shapes of the composite particles are not so clear-cut in comparison to the

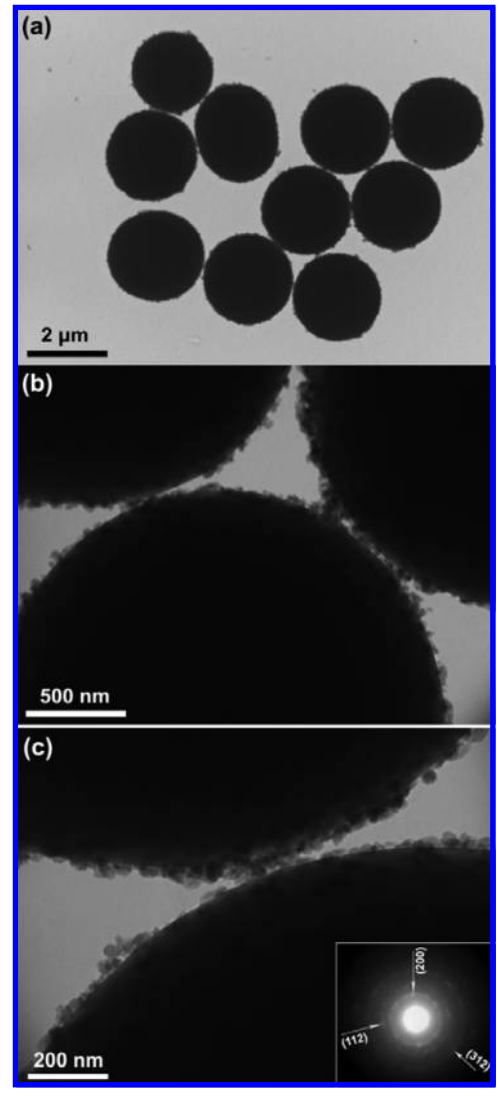

Figure 5. Low- (a) and high-magnification (b, c) TEM images of $MF/YVO_4:Eu^{3+}$ composite microspheres prepared at 70 °C. Inset in (c) is the SAED pattern taken from the nanocrystals on the surface of MF microspheres.

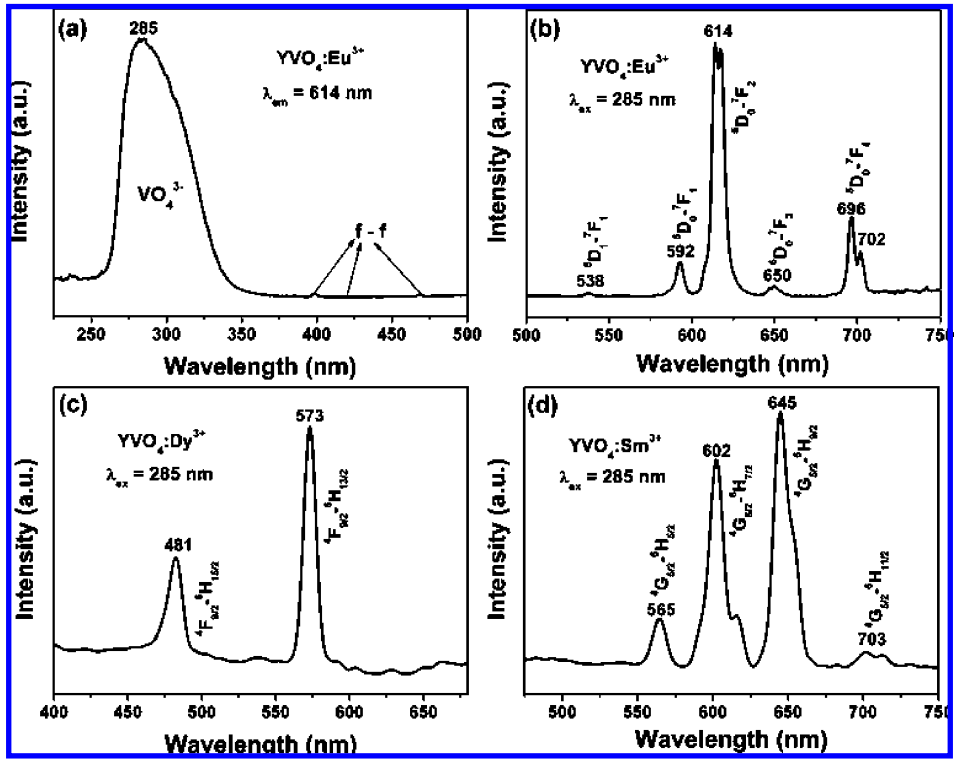

Figure 6. (a) Excitation and (b) emission spectra of as-obtained MF/YVO_4:Eu^{3+} phosphor; emission spectra of (c) MF/YVO_4:Dy^{3+} and (d) MF/YVO_4:Sm^{3+} samples upon excitation at 285 nm.

sample prepared at 70 °C. The morphological change after increasing the reaction temperature can be explained as follows: at given reaction conditions, an increase of the reaction temperature increases the rates of nucleation and growth of YVO_4 nanoparticles significantly. Consequently, more YVO_4 begin to nucleate and grow in a short time, leading to the dense and concentrated deposition on the template surface.

To provide further insight into the MF/YVO_4 composite particles, TEM investigation was also performed. Figure 5a displays a typical TEM image of MF/YVO_4 composite microspheres prepared at 70 °C. It can be observed that the as-prepared composite sample is composed of uniform spherical particles with an average size of 2.5 μm, and these particles are nonaggregated with narrow size distribution. From the high-magnification TEM images (Figure 5b,c), it can be seen clearly that the YVO_4 nanoparticles are distributed on the surface of MF microspheres uniformly. The results are in agreement with the SEM observations presented above (Figure 4c,d). The corresponding selected-area electron diffraction (SAED) pattern (inset in Figure 5c), taken from the YVO_4 nanoparticles on the surface of MF template, shows diffuse rings, indicating that the YVO_4 nanoparticles are polycrystalline. The concentric rings from inside to outside could be well indexed to (200), (112), and (312) planes of tetragonal phase YVO_4, respectively.[32,33]

3.2. Luminescence Properties of MF/YVO_4:Ln^{3+} Phosphors. Figure 6a,b shows the excitation and emission spectra of the MF/YVO_4:Eu^{3+} composite particles. The excitation spectrum (Figure 6a) consists of a strong absorption band with a maximum at 285 nm and several weak lines. The strong absorption band is due to the charge transfer from the oxygen ligands to the central vanadium ions inside the VO_4^{3-} groups. The weak lines are attributed to the f−f transitions within the $4f^6$ configuration of the Eu^{3+} ions. The absorption intensity of the general f−f transitions of the Eu^{3+} ions in the longer wavelength region is very weak in comparison with that of the VO_4^{3-} groups, indicating that the excitation of the Eu^{3+} ions is mainly through the VO_4^{3-} groups. The emission spectrum (Figure 6b) exhibits five groups of emission lines at about 538, 592, 614 (617), 650, and 696 (702) nm, which are ascribed to the $^5D_1-{}^7F_1$ and $^5D_0-{}^7F_J$ ($J = 1, 2, 3, 4$) transitions of the Eu^{3+} ions, respectively. No emission from the VO_4^{3-} groups was observed, revealing that the energy transfer from the VO_4^{3-} groups to Eu^{3+} ions is very efficient. The emission spectrum is dominated by the red $^5D_0-{}^7F_2$ (614 nm) transition of the Eu^{3+} ions, due to an electric-dipole allowed transition of the Eu^{3+} ions in YVO_4. The excitation spectra of MF/YVO_4:Dy^{3+} and MF/YVO_4:Sm^{3+} composite samples are very similar to the MF/YVO_4:Eu^{3+} sample (not shown). Upon excitation at 285 nm, the emission spectra of MF/YVO_4:Dy^{3+} and MF/YVO_4:Sm^{3+} samples are shown in Figure 6c,d, respectively. There are two dominant bands in the emission spectrum of the Dy^{3+}-doped sample (Figure 6c). The yellow band (573 nm) corresponds to the $^4F_{9/2}-{}^6H_{13/2}$ transition and the blue band (481 nm) corresponds to the $^4F_{9/2}-{}^6H_{15/2}$ transition of Dy^{3+} ions. The emission intensity of most f−f transitions of trivalent rare-earth ions is little affected by the local surroundings of the ions. However, the emission intensity of some transitions is very sensitive to the local environments of the ions. Such transitions are called hypersensitive transitions and they would follow the selection rules as $\Delta J \leq 2$, $\Delta L \leq 2$, $\Delta S = 0$.[34] In the observable emission bands of the Dy^{3+} ions, the emission band of the $^4F_{9/2}-{}^6H_{13/2}$ transition is the hypersensitive transition, being sensitive to the local surroundings of the Dy^{3+} ions. Excitation into the orthovanadate groups at 285 nm yields the characteristic emission of the Sm^{3+} ions at 565 nm ($^4G_{5/2}-{}^6H_{5/2}$), 602 nm ($^4G_{5/2}-{}^6H_{7/2}$), 645 nm ($^4G_{5/2}-{}^6H_{9/2}$), and 703 (715) nm ($^4G_{5/2}-{}^6H_{11/2}$) due to an energy transfer from the VO_4^{3-} groups to Sm^{3+} ions (Figure 6d). The emission band of YVO_4 was not

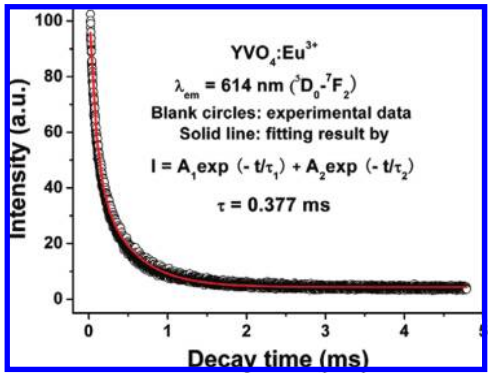

Figure 7. Decay curve for the $^5D_0-^7F_2$ (614 nm) emission of Eu^{3+} in MF/YVO_4:Eu^{3+} sample.

observed, indicating that the host can transfer its absorbed energy to the activators efficiently.

The representative decay curve for the luminescence of the Eu^{3+} ions in the MF/YVO_4:Eu^{3+} core−shell structured phosphor is shown in Figure 7. The decay curve for the luminescence of the Eu^{3+} ions (monitored by $^5D_0-^7F_2$, 614 nm) can be well fitted into a double-exponential function as $I = A_1 \exp(-t/\tau_1) + A_2 \exp(-t/\tau_2)$, in which τ is the decay lifetime.[33] The average lifetime of Eu^{3+} in YVO_4 host lattices is determined to be 0.377 ms. This result is basically in agreement with the previous reports given for the YVO_4:Eu^{3+} nanoparticles.[6,17,33]

4. Conclusions

A facile and general method has been successfully developed to fabricate MF/YVO_4:Ln^{3+} (Ln = Eu, Dy, and Sm) composite phosphors. The morphology, crystal structure, element analysis, and luminescence properties were characterized by XRD, FT-IR, EDX, SEM, TEM, PL, and kinetic decays, respectively. SEM and TEM images indicate that the obtained composite particles are nonaggregated and highly uniform in size and distribution. The possible mechanism for the formation of the core−shell structure has been discussed in detail. Under ultraviolet excitation, the as-prepared MF/YVO_4:Ln^{3+} composite phosphors show strong light emissions with different colors coming from different activator ions. Furthermore, this simple and efficient method may be of significance in the synthesis of many other core−shell structured luminescent materials with spherical morphology and may decrease the cost of phosphors to some degree because melamine formaldehyde resin is much cheaper than most of the phosphor materials.

Acknowledgment. This work is financially supported by the National Natural Science Foundation of China (Grant No. 20771098) and the National Basic Research Program of China (973 Program, Grant Nos. 2007CB935502).

References

(1) Chen, M. H.; Gao, L.; Yang, S. W.; Sun, J. *Chem. Commun.* **2007**, *12*, 1272.
(2) Ow, H.; Larson, D. R.; Srivastava, M.; Baird, B. A.; Webb, W. W.; Wiesner, U. *Nano Lett.* **2005**, *5*, 113.
(3) Rogach, A.; Susha, A.; Caruso, F.; Sukhorukov, G.; Kornowski, A.; Kershaw, S.; Mohwald, H.; Eychmuller, A.; Weller, H. *Adv. Mater.* **2000**, *12*, 333.
(4) Nair, A. S.; Tom, R. T.; Suryanarayanan, V.; Pradeep, T. *J. Mater. Chem.* **2003**, *13*, 297.
(5) Chang, M. L.; Tie, S. L. *Nanotechnology* **2008**, *19*, 075711.
(6) Lu, Y.; Yin, Y.; Li, Z. Y.; Xia, Y. *Nano Lett.* **2002**, *2*, 785.
(7) Suryanarayanan, V.; Nair, A. S.; Tom, R. T.; Pradeep, T. *J. Mater. Chem.* **2004**, *14*, 2661.
(8) Caruso, F. *Adv. Mater.* **2001**, *13*, 11.
(9) Chan, Y.; Zimmer, J. P.; Stroh, M.; Steckel, J. S.; Jain, R. K.; Bawendi, M. G. *Adv. Mater.* **2004**, *16*, 2092.
(10) Schärtl, W. *Adv. Mater.* **2000**, *12*, 1899.
(11) Tissot, I.; Reymond, J. P.; Lefebvre, F.; Bourgeat-Lami, E. *Chem. Mater.* **2002**, *14*, 1325.
(12) Sherman, R. L.; Ford, W. T. *Langmuir* **2005**, *21*, 5218.
(13) Agrawal, M.; Pich, A.; Zafeiropoulos, N. E.; Gupta, S.; Pionteck, J.; Simon, F.; Stamm, M. *Chem. Mater.* **2007**, *19*, 1845.
(14) Zhong, Z.; Yin, Y.; Gates, B.; Xia, Y. *Adv. Mater.* **2000**, *12*, 206.
(15) Caruso, F.; Spasova, M.; Susha, A.; Giersig, M.; Caruso, R. A. *Chem. Mater.* **2001**, *13*, 109.
(16) Lin, C. K.; Kong, D. Y.; Liu, X. M.; Wang, H.; Yu, M.; Lin, J. *Inorg. Chem.* **2007**, *46*, 2674.
(17) Yu, M.; Lin, J.; Fang, J. *Chem. Mater.* **2005**, *17*, 1783.
(18) Choi, W. S.; Koo, H. Y.; Kim, D. Y. *Langmuir* **2008**, *24*, 4633.
(19) Choi, W. S.; Koo, H. Y.; Kim, D. Y. *Adv. Mater.* **2007**, *19*, 451.
(20) Friedel, B.; Greulich-Weber, S. *Small* **2006**, *2*, 859.
(21) Li, W. R.; Chen, D. H.; Li, Z.; Shi, Y. F.; Wan, Y.; Wang, G.; Jiang, Z. Y.; Zhao, D. Y. *Carbon* **2007**, *45*, 1757.
(22) Choi, W. S.; Koo, H. Y.; Huck, W. T. S. *J. Mater. Chem.* **2007**, *17*, 4943.
(23) Zheng, S. P.; Tao, C.; He, Q.; Zhu, H. F.; Li, J. L. *Chem. Mater.* **2004**, *16*, 3677.
(24) Kato, N.; Schuetz, P.; Fery, A.; Caruso, F. *Macromolecules* **2002**, *35*, 9780.
(25) Kang, Y. C.; Lenggoro, I. W.; Park, S. B.; Okuyama, K. *Mater. Res. Bull.* **2000**, *35*, 789.
(26) Jing, X.; Ireland, T. G.; Gibbons, C.; Barber, D. J.; Silver, J.; Vecht, A.; Fern, G.; Trogwa, P.; Morton, D. *J. Electrochem. Soc.* **1999**, *146*, 4546.
(27) Cho, S. H.; Yoo, J. S.; Lee, J. D. *J. Electrochem. Soc.* **1998**, *145*, 1017.
(28) Celikkaya, A.; Akinc, M. *J. Am. Ceram. Soc.* **1990**, *73*, 2360.
(29) Gao, C. Y.; Moya, S.; Lichtenfeld, H.; Casoli, A.; Fiedler, H.; Donath, E.; Möhwald, H. *Macromol. Mater. Eng.* **2001**, *286*, 355.
(30) Wang, H.; Yu, M.; Lin, C. K.; Lin, J. *J. Colloid Interface Sci.* **2006**, *300*, 176.
(31) Sun, Y. J.; Liu, H. J.; Wang, X.; Kong, X. G.; Zhang, H. *Chem. Mater.* **2006**, *18*, 2726.
(32) Wang, Y. H.; Zuo, Y. Y.; Gao, H. *Mater. Res. Bull.* **2006**, *41*, 2147.
(33) Jia, G.; Song, Y. H.; Yang, M.; Huang, Y. J.; Zhang, L. H.; You, H. P. *Opt. Mater.* **2009**, *31*, 1032.
(34) Jørgensen, C. K.; Judd, B. R. *Mol. Phys.* **1964**, *8*, 281.

CG9004104